Metalloenzymes

International Edition: DOI: 10.1002/anie.201511896
German Edition: DOI: 10.1002/ange.201511896

[FeFe]-Hydrogenase with Chalcogenide Substitutions at the H-Cluster Maintains Full H_2 Evolution Activity

Jens Noth, Julian Esselborn, Jörn Güldenhaupt, Annika Brünje, Anne Sawyer, Ulf-Peter Apfel, Klaus Gerwert, Eckhard Hofmann, Martin Winkler, and Thomas Happe**

Abstract: *The [FeFe]-hydrogenase HYDA1 from Chlamydomonas reinhardtii is particularly amenable to biochemical and biophysical characterization because the H-cluster in the active site is the only inorganic cofactor present. Herein, we present the complete chemical incorporation of the H-cluster into the HYDA1-apoprotein scaffold and, furthermore, the successful replacement of sulfur in the native [4Fe$_H$] cluster with selenium. The crystal structure of the reconstituted pre-mature HYDA1-[4Fe4Se]$_H$ protein was determined, and a catalytically intact artificial H-cluster variant was generated upon in vitro maturation. Full hydrogen evolution activity as well as native-like composition and behavior of the redesigned enzyme were verified through kinetic assays, FTIR spectroscopy, and X-ray structure analysis. These findings reveal that even a bioinorganic active site with exceptional complexity can exhibit a surprising level of compositional plasticity.*

With turnover frequencies of up to 10^4 molecules of dihydrogen (H_2) per second, [FeFe]-hydrogenases are the fastest known biocatalysts for the reduction of protons to H_2.[1] There are several types of [FeFe]-hydrogenases, which differ not only in protein structure and composition, but also in the number of accessory [FeS]-clusters, which act as an electron (e^-) relay between the e^--mediator docking site and the active center (H-cluster) of the enzyme.[2] The H-cluster is a complex inorganic cofactor, consisting of a cysteine-coordinated [4Fe4S]-cluster ([4Fe$_H$]) linked to a unique [2Fe2S]-subcluster ([2Fe$_H$]) with three CO and two CN^- ligands. An azadithiolate (adt =-S-CH_2-NH-CH_2-S-) ligand, bridging both Fe sites in [2Fe$_H$] (proximal (Fe$_p$) and distal (Fe$_d$) relative to the [4Fe$_H$]-moiety) is essential for fast proton shuttling to and from the vacant ligand site at Fe$_d$,[3] where proton reduction and H_2 oxidation occur (Figure 1 A).[1c,4] Owing to its structural simplicity, the monomeric hydrogenase, HYDA1, from the unicellular green alga *Chlamydomonas reinhardtii*, is a model enzyme for studying the catalytic features of [FeFe]-hydrogenases. As the H-cluster is the only bioinorganic cofactor in the algal enzyme, spectroscopy can be used to directly probe its metal cofactor. Furthermore, HYDA1 can be efficiently expressed and purified with high yields in *Escherichia coli*.[5] While standard [FeS]-clusters, including the [4Fe$_H$]-moiety of the H-cluster, can be synthesized in vivo by housekeeping iron–sulfur cluster biosynthetic machineries,[6] the formation of the unique [2Fe$_H$]-subsite depends on the three highly specific maturation factors, HYDE, -F, and -G.[7] Recently, we found that the complex maturation pathway, which does not natively occur in *E. coli*, can be bypassed in vitro by adding the synthetic [2Fe$_H$]-analogue [$Fe_2(CO)_4$-$(CN)_2$(adt)]$^{2-}$ ([2Fe$_H$]^{MIM}) to the inactive pre-mature HYDA1[4Fe$_H$], rapidly yielding a fully functional enzyme.[3a,b]

In the present study, we applied this tool of in vitro maturation, in combination with the technique of chemical [FeS]-cluster reconstitution,[8] to demonstrate that H-cluster manipulation is not confined to the [2Fe$_H$]-site,[3a,b] but can be extended to the [4Fe$_H$]-moiety, thus enabling the artificial synthesis and manipulation of the complete H-cluster architecture.

The [2Fe$_H$]- and the [4Fe$_H$]-cluster play synergistic roles in the catalytic cycle of the H-cluster. Both subsites are coupled by only one bridging cysteine ligand, resulting in a functional unit through which electrons are reversibly shuttled between the location of substrate turnover at Fe$_d$ and external e^--mediators that dock at the entrance of the e^--relay ([4Fe$_H$]) (Figure 1 A).[9] In 2009, chemical reconstitution was shown for the first time for the biosynthesized *C. reinhardtii* HYDA1 [4Fe$_H$] cubane cluster, further denoted as [4Fe4S]$_H$.[10] Two concurrent studies revealed that a pre-formed cubane cluster is essential for HYDF-mediated incorporation of the [2Fe$_H$]-subsite into HYDA1. As the tertiary protein structure folds around the cubane cluster, the essential framework is prepared for the functional incorporation of the substrate-binding [2Fe$_H$]-cluster. The redox features and protonation state of the [2Fe$_H$]-subcluster change while passing through the catalytic steps of the turnover cycle. Three main catalytic

[*] Dr. J. Noth, Dr. J. Esselborn, A. Brünje, Dr. A. Sawyer, Dr. M. Winkler, Prof. T. Happe
Ruhr Universität Bochum
Lehrstuhl für Biochemie der Pflanzen, AG Photobiotechnologie
Universitätsstrasse 150, 44801 Bochum (Germany)
E-mail: thomas.happe@ruhr-uni-bochum.de
Dr. J. Güldenhaupt, Prof. K. Gerwert
Ruhr Universität Bochum
Lehrstuhl für Biophysik, AG Spektroskopie
Universitätsstrasse 150, 44801 Bochum (Germany)
Prof. E. Hofmann
Ruhr Universität Bochum
Lehrstuhl für Biophysik, AG Röntgenstrukturanalyse an Proteinen
Universitätsstrasse 150, 44801 Bochum (Germany)
Dr. U.-P. Apfel
Ruhr Universität Bochum
Fakultät für Chemie und Biochemie
Lehrstuhl für Anorganische Chemie I/ Bioanorganische Chemie
Universitätsstrasse 150, 44801 Bochum (Germany)
E-mail: ulf.apfel@ruhr-uni-bochum.de

Supporting information for this article can be found under: http://dx.doi.org/10.1002/anie.201511896.

states are clearly distinguishable by infrared spectroscopy. The crucial participation of the $[4Fe_H]$-site in the catalytic cycle became obvious after the discovery that the two-fold reduced H_{sred} state is part of the reaction mechanism, which unlike H_{ox} and H_{red}, exhibits a reduced $[4Fe_H]$-site.[4,11] Therefore, in contrast to other reported examples of chalcogenide replacement in [FeS]-clusters, such as those of plant type and bacterial ferredoxins,[12] the $[4Fe_H]$-cluster targeted here is an essential part of the catalytic cofactor itself.

Cluster-free HYDA1[ΔH] was prepared by removing the in-vivo-incorporated $[4Fe_H]$-cluster from native HYDA1-$[4Fe_H]$. This HYDA1[ΔH], as shown previously,[10] did not display catalytic H_2-production activity upon addition of $[2Fe_H]^{MIM}$ (Figure 1B). This allowed us to monitor time-resolved $[4Fe_H]$-cluster reconstitution by measuring enzyme activity after in vitro activation with synthesized $[2Fe_H]^{MIM}$ (Figure 1B).

HYDA1[ΔH] reconstitution mixtures in which only Fe^{2+} or one of the chalcogenides (S^{2-} or Se^{2-}) were added did not reveal any significant H_2 evolution activity (< 3% compared to Fe^{2+}/S^{2-}-reconstituted HYDA1 (HYDA1$[4Fe4S]_H$)) upon addition of $[2Fe_H]^{MIM}$, indicating the successful removal of the bio-assembled $[4Fe_H]$ during preparation of HYDA1[ΔH] (Figure 1B). Notably, reconstitution mixtures containing HYDA1[ΔH], in combination with Fe^{2+} and either S^{2-} or Se^{2-}, exhibited strongly increasing H_2 production activities over time upon in vitro maturation, with maximum rates occurring after 19 h (Figure 1B). In comparison to the Fe^{2+}/S^{2-} samples, the reconstitution kinetics for cluster assembly of the Fe^{2+}/Se^{2-} combination were slightly slower in the first hours. However, the maximum specific activity after in vitro maturation did not deviate significantly from that observed after reconstitution with Fe^{2+} and S^{2-} (Figure 1B,C). Upon reconstitution with Fe^{2+} and either S^{2-} or Se^{2-}, activities of almost 600 μmol H_2 min^{-1} mg^{-1} were achieved (Figure 1B). Our results suggest that the chemical self-assembly of the $[4Fe4X]_H$ cluster (X = S, Se) is a slow process compared to the subsequent spontaneous activation of HYDA1$[4Fe_H]$ by chemically synthesized $[2Fe_H]^{MIM}$.[3a,b] However, differences in reaction kinetics are expected, as complete $[4Fe4X]_H$ assembly involves protein folding and passes through several metal cluster intermediates.[8a] In contrast, incorporation of $[2Fe_H]^{MIM}$ only requires the formation of a single covalent bond and subsequent CO dissociation.[3a,b] After 19 h of cluster reconstitution, H_2-production activities of samples from $[2Fe_H]^{MIM}$-activated crude mixtures for both cluster types reached 60% of the activity detected for the control sample of in vitro maturated HYDA1$[4Fe_H]$ expressed in *E. coli*. However, upon additional protein purification between reconstitution and in vitro maturation, which removes misfolded and aggregated HYDA1[ΔH], specific activities of both enzyme variants (HYDA1$[4Fe4Se]_H^{MIM}$ and HYDA1$[4Fe4S]_H^{MIM}$) reached 85% of the wild-type activity (Figure 1C). Thus, replacing S^{2-} with Se^{2-} still allows for the subsequent incorporation of $[2Fe_H]^{MIM}$ and, moreover, does not alter the catalytic features of the H-cluster.

The kinetic parameters of the two chemically reconstituted HYDA1$[4Fe4X]_H^{MIM}$ proteins were determined using both the artificial e^--mediator methyl viologen (MV) and the native redox partner ferredoxin (PETF; Supporting Information, Figure S1 and Table S1). Both mediators are assumed to directly transfer electrons to the $[4Fe_H]$ cluster of HYDA1.[13] The K_m and V_{max} values were similar to those from in vivo assembled HYDA1$[4Fe_H]$ with synthetic $[2Fe_H]^{MIM}$ cluster[3b] and correspond to previously published data for wild-type HYDA1.[13b,14,15] To verify the successful chalcogenide exchange in reconstituted HYDA1$[4Fe4Se]_H$, the protein was crystallized under anaerobic conditions and its structure determined using HYDA1$[4Fe_H]$ (PDB ID 3LX4) as a reference model.[16] The crystal structure allowed us to confirm the consistency of the overall protein structure with the native enzyme. Although the resolution of 3.1 Å was not sufficient to determine deviations in cluster geometry, or the exact distances between Fe and chalcogenide atoms in reference

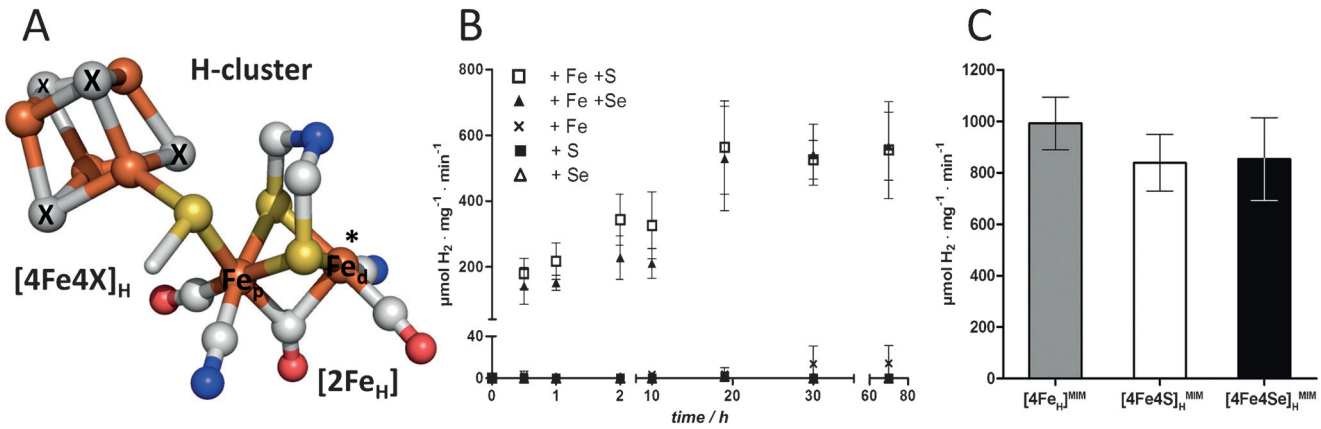

Figure 1. Cluster incorporation and specific H_2-production rates of HYDA1 holoenzymes with S- and Se-reconstituted H-clusters. A) Ball and stick model of the chalcogenide-substituted cubane subcluster $[4Fe4X]_H$ as part of the H-cluster consisting of $[4Fe4X]_H$ (X = S, Se; gray) and $[2Fe_H]$ (PDB ID 3C8Y). *location of catalytic turnover. B) Time-dependency of the chemical HYDA1 $[4Fe4X]_H$ cubane cluster reconstitution by determination of the specific H_2-production rates of the in vitro maturated holoenzymes. Reconstitution reactions contained iron (Fe^{2+}) and either sulfide (S^{2-}) or selenide (Se^{2-}), while control mixtures only contained Fe^{2+}, S^{2-}, or Se^{2-} as indicated. C) For determining the specific H_2-production activity, 10 nM of overnight (19 h)-reconstituted and purified HYDA1$[4Fe4X]_H$ enzyme was measured compared to wild-type (HYDA1$[4Fe_H]$) with a 10-fold excess of $[2Fe_H]^{MIM}$. All experiments were performed in triplicate and error bars represent the standard deviation.

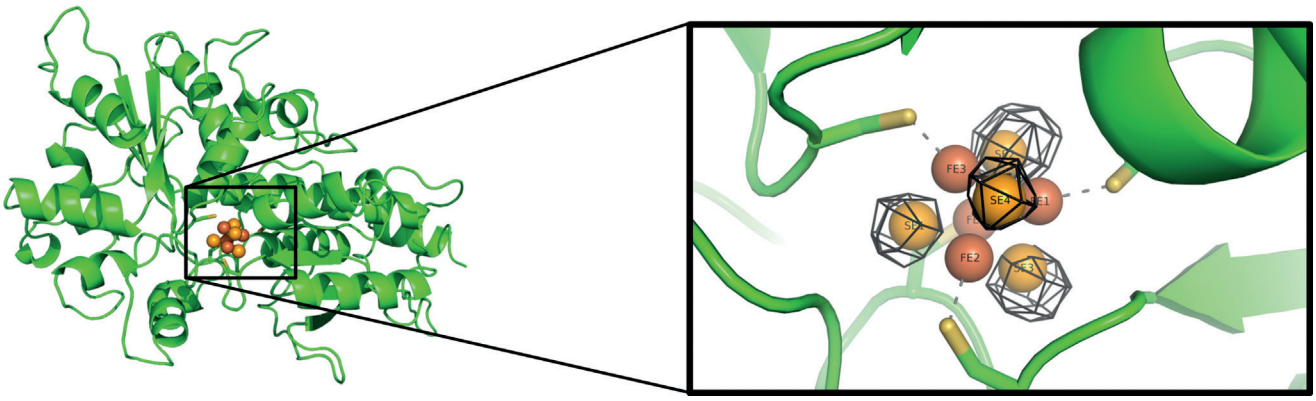

Figure 2. Crystal structure of HYDA1[4Fe4Se]$_H$ and localization of Se atoms in the cubane cluster. Presented is a cartoon model of the HYDA1[4Fe4Se]$_H$ structure at a resolution of 3.1 Å. A detailed view of the [4Fe4Se]$_H$ cubane cluster is shown in the magnification with the Se anomalous electron density presented as a mesh. Selenide atoms were located at the sulfur positions of the reference cluster by calculating a difference map (black mesh; contoured at 6 σ) of the anomalous difference Fourier maps from datasets on and below the absorption edge of Se (protein backbone, green; Fe, brown; Se, ochre; cysteinyls, yellow).

to the standard [4Fe$_H$]-cluster, selenide atoms could be unambiguously located at the sulfide positions of the native reference cluster (PDB ID 3LX4) owing to the strong anomalous scattering of selenide at 12.666 keV (Figure 2 and Figure S2). To yield a selenium-specific anomalous difference Fourier map, single-crystal measurements of the anomalous signal on and below the Se K-edge were subtracted. The electron densities of this difference map did not significantly deviate from one cubane edge to another, indicating a homogeneous occupancy of Se atoms at all four cluster positions (Figure S3). Successful chalcogenide exchange was previously reported for the [4Fe4S]-cluster in dinitrogenase reductase (Fe-protein) of *Klebsiella pneumoniae*.[12c] However, the resulting [4Fe4Se]-protein exhibited a five-fold decrease in ATP-specific e$^-$-transfer rate compared to the native dinitrogenase, leading to an overall 20-fold reduction in specific activity. It was therefore possible that the chalcogenide exchange here could alter the redox properties of the [FeS]-clusters. This was found to be the case for ferredoxins,[17] as well as for a model complex of the [2Fe$_H$] with selenium-substituted acid-labile sulfur atoms.[18] The HYDA1 [4Fe$_H$]-cluster is a redox-active catalytic cofactor, thus any redox change to the cluster would also change the redox-dependent catalytic features of the enzyme. For example, for the radical SAM protein biotin synthase, the replacement of sulfur with selenide within the two iron–sulfur sites (the [4Fe4S]-cluster that coordinates and reduces S-adenosyl-methionine and the [2Fe2S]-cluster that donates sulfur for biotin formation) severely reduced the turnover of biotin synthesis by 70 %.[19] To determine whether the redox properties of the [2Fe$_H$]-subcluster were affected here, Fourier transform infrared (FTIR) spectroscopy was performed. FTIR spectroscopy can detect minor deviations in the structural arrangement as well as electron distribution of the [FeFe]-hydrogenase active site, which are reflected by shifts of absorbance bands in the vibrational spectrum of the Fe-C(=O/N) ligands in the [2Fe$_H$]-subcluster (Figure 1 A).[1c,4,11,20] Accordingly, FTIR-measurements were conducted with both chalcogenide-reconstituted and in-vitro-maturated HYDA1[4Fe4X]$_H^{MIM}$, and wild-type HYDA1-[4Fe$_H$]^{MIM}. HYDA1 samples were converted to characteristic catalytic and non-catalytic states. To enable a spectral comparison of both reconstituted proteins to HYDA1[4Fe$_H$]^{MIM} in an unambiguously defined state, the three proteins were purged with 100 % carbon monoxide gas (CO) prior to measurements leading to the homogeneous enrichment of the non-catalytic H$_{ox}$-CO state (Figure 3 a, b).[4,11,20] Purging with N_2 led to a mixture of the three described catalytic resting states: H$_{ox}$, the oxidized ready state, and the two reduced states, H$_{red}$ and H$_{sred}$[4,11] (Figure 3 c). A selective accumulation of H$_{ox}$ was achieved by addition of thionine (Figure 3 d). Although all of the protein samples showed fractions of H$_{ox}$-CO, the specific CO and CN$^-$ vibration signals for H$_{ox}$ and both reduced states in HYDA1[4Fe4Se]$_H^{MIM}$ fully matched the corresponding band positions of the respective control samples (Figure 3; Table S3).

The FTIR spectra thus confirmed both the stable incorporation of [2Fe$_H$]^{MIM} into reconstituted HYDA1[4Fe4X]$_H$ proteins and an unaltered [2Fe$_H$]-ligand coordination/electron distribution of non-catalytic and catalytic states compared to wild-type HYDA1[4Fe$_H$]^{MIM} (Figure 3).[3b,4] Upon comparison of the absorbance of the bridging CO (1820–1800 cm^{-1}) in H$_{ox}$-CO with the integral of the amide II band (1600–1485 cm^{-1}, omitted in Figure 3 for clarity), which was used as a measure of protein concentration, it was determined that [2Fe$_H$]^{MIM} had an occupancy of 61 % in HYDA1-[4Fe4S]$_H^{MIM}$ and 77 % in HYDA1[4Fe4Se]$_H^{MIM}$ compared to HYDA1[4Fe$_H$]^{MIM}. Di-iron-cluster occupancy and specific activities of the purified in vitro maturated HYDA1-[4Fe4X]$_H^{MIM}$ proteins were comparable and further corresponded to the features of the control sample, confirming that in vitro maturation of HYDA1[4Fe4Se]$_H$ indeed results in a fully active variant of the unique and complex H-cluster. The results presented here, together with those from other recently published works,[3b,21] demonstrate that both H-cluster parts can be derivatized without destroying catalytic activity. The fact that a [4Fe4Se]-cluster, as part of the H-cluster, displays full catalytic activity is of particular interest. It is well known from synthetic [4Fe4X(SR)$_4$]$^{3-}$ (X = S, Se) cubanes that S and Se homologs show only small differences

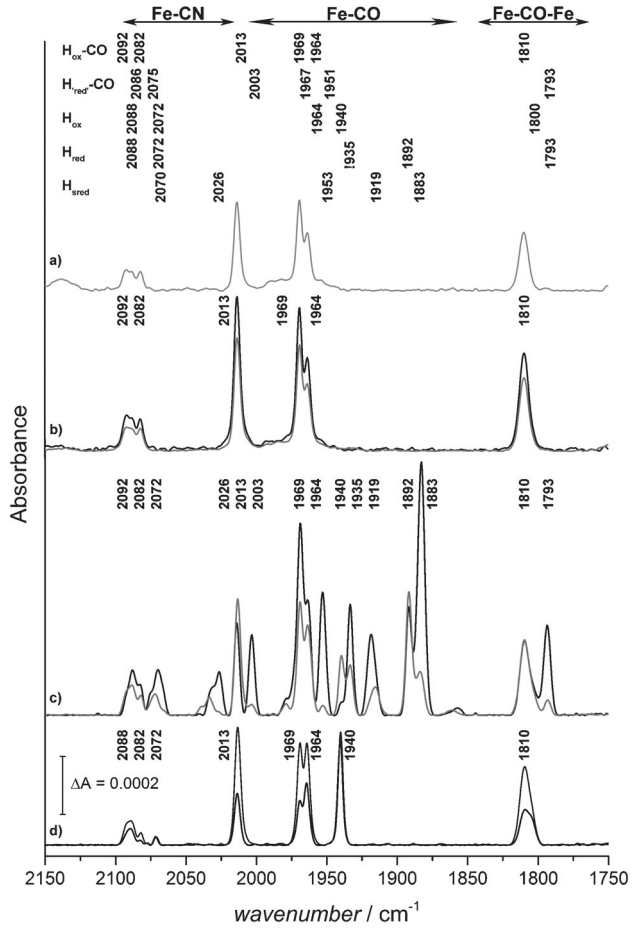

Figure 3. FTIR measurements of HYDA1[4Fe4X]$_H^{MIM}$ in comparison to HYDA1[Fe$_H$]^{MIM}. Comparison of state-enriched CO/CN-ligand spectra of the [2Fe$_H$]-subsite of wild-type protein and HYDA1 samples with reconstituted and maturated H-cluster, normalized to the amide II signal of HYDA1[4Fe$_H$]^{MIM} and vertically displaced for clarity. a) HYDA1[4Fe4S]$_H^{MIM}$ (150 μM) flushed with 100% CO prior to FTIR measurement to generate the defined H_{ox}-CO state of the [2Fe$_H$]-cofactor. b) HYDA1[4Fe4Se]$_H^{MIM}$ (300 μM) red and HYDA1[4Fe$_H$]^{MIM} (150 μM) in black prepared as described for (a). c) HYDA1[4Fe4Se]$_H^{MIM}$ (420 μM) and HYDA1[4Fe$_H$]^{MIM} (300 μM) after flushing with 100% N_2. d) HYDA1[4Fe4Se]$_H^{MIM}$ (330 μM) and HYDA1[4Fe$_H$]^{MIM} (300 μM) oxidized with a 3-fold molar excess of thionine. State-annotation was adapted from Ref. [11].

in their basic structures, with the average Fe–Se bond being slightly larger ($\approx$0.12 Å) compared to the Fe–S bond.[22] Comparable force constants also reflect the similarity of the Fe–S and Fe–Se bonds.

Despite structural similarities, the electronic properties can differ significantly, as was shown by cyclic voltammetry on homologous [4Fe4X]-cluster compounds.[22] Notably, [4Fe4Se]-complexes displayed more positive reduction potentials compared to their [4Fe4S] counterparts and were thus easier to reduce. This difference indeed should lead to an altered e^--exchange behavior between the [4Fe4Se]$_H$-cluster and the [2Fe$_H$]-subsite of the H-cluster variant presented here, which again should be reflected in shifted CO/CN^- ligand spectra for the different catalytic states of the latter subsite. This however is not deducible from any of the available experimental data. Instead, the present study shows that selenium can act as a fully-fledged substitute for sulfur yielding a functional [FeFe]-hydrogenase. In addition, we herein provide evidence that the H-cluster tolerates electronic manipulations in the interplay of the [4Fe$_H$]-cluster and the [2Fe$_H$]-subsite. This seems unexpected given the fact that efficient subcluster communication is crucial for fulfilling the catalytic cycle. However, the FTIR-spectra of reduced HYDA1 maturated in vitro with the non-natural derivative $[Fe_2(CO)_4(CN)_2(pdt)]^{2-}$ of the [2Fe$_H$]-cofactor, which does not provide H_2 turnover activity, only showed minor shifts of 3–12 cm^{-1} in the CO/CN^--band pattern compared to the oxidized state.[11] This was attributed to the fact that, unlike the native [2Fe$_H$]-version, this single reduction step is restricted to the [4Fe$_H$]-site. Thus, while both subclusters are functionally coupled, the effect of changes in redox state and constitution of the [4Fe$_H$]- moiety on the catalytic features of the [2Fe$_H$]-site seem to be restricted. It can be assumed that chalcogenide substitution within the [2Fe$_H$]-site will more prominently affect the catalytic features and state-specific FTIR-band patterns as it directly modulates the electronic fine-structure of the actual location of catalytic turnover.

Having now the complementary tools of cubane cluster reconstitution and in vitro [2Fe$_H$]^{MIM} maturation of HYDA1, it is possible to individually label both clusters by site-directed exchange of a particular element within the H-cluster for advanced spectroscopic investigations. Moreover, the complete chemical incorporation allows for the inclusion of the whole H-cluster into next-generation enzyme engineering concepts.

The successful de novo synthesis of a functional H-cluster-type, as described here, will encourage other scientists to add another dimension, and thus level of quality, to their future enzyme design projects going beyond simple modulations in the protein environment.

Acknowledgements

We acknowledge the European Synchrotron Radiation Facility, Grenoble, France and the Paul Scherrer Institut, Villigen, Switzerland for provision of synchrotron radiation facilities, and we would like to thank the staff at beamlines ID29 (ESRF) and PXII (PSI-SLS) for assistance. We are grateful to Dr. Matthias Mueller and Dr. Mandy Miertzschke from the MPI of Molecular Physiology, Dortmund, Germany, for their help during data collection at the Paul Scherrer Institut. T.H. gratefully acknowledges support from the Deutsche Forschungsgemeinschaft (DFG) (DIP project cooperation "Nanoengineered optoelectronics with biomaterials and bioinspired assemblies"; Cluster of Excellence RESOLV, EXC1069), the Volkswagen Foundation (LigH2t), and the EU (Sun2Chem). U.-P.A. thanks the Fonds of the Chemical Industry (Liebig grant) and the Deutsche Forschungsgemeinschaft (Emmy Noether grant, AP242/2-1) for financial support.

Keywords: chalcogenide exchange · H_2 production · H-clusters · hydrogenases · selenium

How to cite: *Angew. Chem. Int. Ed.* **2016**, *55*, 8396–8400
Angew. Chem. **2016**, *128*, 8536–8540

[1] a) C. Madden, M. D. Vaughn, I. Diez-Perez, K. A. Brown, P. W. King, D. Gust, A. L. Moore, T. A. Moore, *J. Am. Chem. Soc.* **2012**, *134*, 1577–1582; b) R. Cammack, *Nature* **1999**, *397*, 214–215; c) W. Lubitz, H. Ogata, O. Rüdiger, E. Reijerse, *Chem. Rev.* **2014**, *114*, 4081–4148; d) K. A. Vincent, A. Parkin, F. A. Armstrong, *Chem. Rev.* **2007**, *107*, 4366–4413.

[2] a) J. Meyer, *Cell. Mol. Life Sci.* **2007**, *64*, 1063–1084; b) P. M. Vignais, B. Billoud, *Chem. Rev.* **2007**, *107*, 4206–4272; c) M. Winkler, J. Esselborn, T. Happe, *Biochim. Biophys. Acta Bioenerg.* **2013**, *1827*, 974–985.

[3] a) G. Berggren, A. Adamska, C. Lambertz, T. R. Simmons, J. Esselborn, M. Atta, S. Gambarelli, J. M. Mouesca, E. Reijerse, W. Lubitz, T. Happe, V. Artero, M. Fontecave, *Nature* **2013**, *499*, 66–69; b) J. Esselborn, C. Lambertz, A. Adamska-Venkatesh, T. Simmons, G. Berggren, J. Noth, J. Siebel, A. Hemschemeier, V. Artero, E. Reijerse, M. Fontecave, W. Lubitz, T. Happe, *Nat. Chem. Biol.* **2013**, *9*, 607–609; c) D. W. Mulder, M. W. Ratzloff, M. Bruschi, C. Greco, E. Koonce, J. W. Peters, P. W. King, *J. Am. Chem. Soc.* **2014**, *136*, 15394–15402.

[4] A. Adamska, A. Silakov, C. Lambertz, O. Rüdiger, T. Happe, E. Reijerse, W. Lubitz, *Angew. Chem. Int. Ed.* **2012**, *51*, 11458–11462; *Angew. Chem.* **2012**, *124*, 11624–11629.

[5] a) J. Noth, R. Kositzki, K. Klein, M. Winkler, M. Haumann, T. Happe, *Sci. Rep.* **2015**, *5*, 13978; b) J. M. Kuchenreuther, C. S. Grady-Smith, A. S. Bingham, S. J. George, S. P. Cramer, J. R. Swartz, *PLoS ONE* **2010**, *5*, e15491.

[6] a) R. Lill, U. Mühlenhoff, *Annu. Rev. Biochem.* **2008**, *77*, 669–700; b) R. Lill, *Nature* **2009**, *460*, 831–838; c) B. Roche, L. Aussel, B. Ezraty, P. Mandin, B. Py, F. Barras, *Biochim. Biophys. Acta Bioenerg.* **2013**, *1827*, 923–937.

[7] a) J. B. Broderick, A. S. Byer, K. S. Duschene, B. R. Duffus, J. N. Betz, E. M. Shepard, J. W. Peters, *J. Biol. Inorg. Chem.* **2014**, *19*, 747–757; b) E. M. Shepard, F. Mus, J. N. Betz, A. S. Byer, B. R. Duffus, J. W. Peters, J. B. Broderick, *Biochemistry* **2014**, *53*, 4090–4104; c) J. M. Kuchenreuther, W. K. Myers, D. L. Suess, T. A. Stich, V. Pelmenschikov, S. A. Shiigi, S. P. Cramer, J. R. Swartz, R. D. Britt, S. J. George, *Science* **2014**, *343*, 424–427.

[8] a) H. Beinert, R. H. Holm, E. Münck, *Science* **1997**, *277*, 653–659; b) R. Malkin, J. C. Rabinowitz, *Biochem. Biophys. Res. Commun.* **1966**, *23*, 822–827.

[9] a) A. S. Pandey, T. V. Harris, L. J. Giles, J. W. Peters, R. K. Szilagyi, *J. Am. Chem. Soc.* **2008**, *130*, 4533–4540; b) J. W. Peters, W. N. Lanzilotta, B. J. Lemon, L. C. Seefeldt, *Science* **1998**, *282*, 1853–1858.

[10] a) D. W. Mulder, D. O. Ortillo, D. J. Gardenghi, A. V. Naumov, S. S. Ruebush, R. K. Szilagyi, B. Huynh, J. B. Broderick, J. W. Peters, *Biochemistry* **2009**, *48*, 6240–6248; b) J. M. Kuchenreuther, J. A. Stapleton, J. R. Swartz, *PLoS One* **2009**, *4*, e7565.

[11] A. Adamska-Venkatesh, D. Krawietz, J. Siebel, K. Weber, T. Happe, E. Reijerse, W. Lubitz, *J. Am. Chem. Soc.* **2014**, *136*, 11339–11346.

[12] a) W. H. Orme-Johnson, R. E. Hansen, H. Beinert, J. C. Tsibris, R. C. Bartholomaus, I. C. Gunsalus, *Proc. Natl. Acad. Sci. USA* **1968**, *60*, 368–372; b) J. Meyer, J. M. Moulis, J. Gaillard, M. Lutz, *Adv. Inorg. Chem.* **1992**, *38*, 73–115; c) P. C. Hallenbeck, G. N. George, R. C. Prince, R. N. Thorneley, *J. Biol. Inorg. Chem.* **2009**, *14*, 673–682.

[13] a) M. Winkler, A. Hemschemeier, J. Jacobs, S. Stripp, T. Happe, *Eur. J. Cell Biol.* **2010**, *89*, 998–1004; b) K. Sybirna, P. Ezanno, C. Baffert, C. Leger, H. Bottin, *Int. J. Hydrogen Energy* **2013**, *38*, 2998–3002; c) S. Rumpel, J. F. Siebel, C. Fares, J. F. Duan, E. Reijerse, T. Happe, W. Lubitz, M. Winkler, *Energy Environ. Sci.* **2014**, *7*, 3296–3301.

[14] a) G. von Abendroth, S. Stripp, A. Silakov, C. Croux, C. Soucaille, L. Girbal, T. Happe, *Int. J. Hydrogen Energy* **2008**, *33*, 6076–6081; b) I. Yacoby, L. T. Tegler, S. Pochekailov, S. Zhang, P. W. King, *PLoS One* **2012**, *7*, e35886.

[15] M. Winkler, S. Kuhlgert, M. Hippler, T. Happe, *J. Biol. Chem.* **2009**, *284*, 36620–36627.

[16] D. W. Mulder, E. S. Boyd, R. Sarma, R. K. Lange, J. A. Endrizzi, J. B. Broderick, J. W. Peters, *Nature* **2010**, *465*, 248–251.

[17] J. M. Moulis, J. Meyer, *Biochemistry* **1982**, *21*, 4762–4771.

[18] R. Trautwein, L. R. Almazahreh, H. Gorls, W. Weigand, *Dalton Trans.* **2015**, *44*, 18780–18794.

[19] B. Tse Sum Bui, T. A. Mattioli, D. Florentin, G. Bolbach, A. Marquet, *Biochemistry* **2006**, *45*, 3824–3834.

[20] A. Silakov, C. Kamp, E. Reijerse, T. Happe, W. Lubitz, *Biochemistry* **2009**, *48*, 7780–7786.

[21] J. F. Siebel, A. Adamska-Venkatesh, K. Weber, S. Rumpel, E. Reijerse, W. Lubitz, *Biochemistry* **2015**, *54*, 1474–1483.

[22] M. A. Bobrik, E. J. Laskowski, R. W. Johnson, W. O. Gillum, J. M. Berg, K. O. Hodgson, R. H. Holm, *Inorg. Chem.* **1978**, *17*, 1402–1410.

Received: December 23, 2015
Revised: March 27, 2016
Published online: May 23, 2016

Angewandte Chemie
Eine Zeitschrift der Gesellschaft Deutscher Chemiker

Supporting Information

[FeFe]-Hydrogenase with Chalcogenide Substitutions at the H-Cluster Maintains Full H_2 Evolution Activity

Jens Noth, Julian Esselborn, Jörn Güldenhaupt, Annika Brünje, Anne Sawyer, Ulf-Peter Apfel, Klaus Gerwert, Eckhard Hofmann, Martin Winkler, and Thomas Happe**

anie_201511896_sm_miscellaneous_information.pdf

This file includes:

SI.1 Detailed experimental procedures

SI.2 Enzyme kinetics of HYDA1[4Fe4X]$_H^{MIM}$ and HYDA1[4Fe$_H$]^{MIM}

SI.3 Supplemental data from crystallography and FTIR of HYDA1[4Fe4Se]$_H$

Supplementary References

SI.1 Detailed experimental procedures

SI 1.1 Heterologous production and purification of HYDA1[4Fe$_H$] and PETF from *C. reinhardtii*.

Heterologous expression of the inactive HYDA1[4Fe$_H$]-pre-form of *Chlamydomonas reinhardtii* was performed in *Escherichia coli* BL21 (DE3) Δ*iscR*.[1] Protein expression and purification were performed according to the previously published procedure.[2] Recombinant [2Fe2S]-ferredoxin (PETF) from *C. reinhardtii* was prepared as described earlier.[3] All purification steps were conducted under strictly anaerobic conditions in an atmosphere of 1-2 % hydrogen in molecular nitrogen.

SI 1.2 Synthesis of disodium selenide for chemical reconstitution of the [4Fe4Se]$_H$ cubane cluster in the bare polypeptide of HYDA1[ΔH].

Attention! Sodium selenide is highly toxic; storage under argon atmosphere is required to avoid the formation of highly toxic H_2Se. Liquid NH_3 should be handled with care as it can expand readily causing severe injuries and damage.

We strongly recommend the use of small amounts of starting materials and the use of an overpressure valve. Incurred wastes need to be collected and disposed separately.

It is mandatory that all glassware is rinsed with an aqueous NaOH solution after use.

In a three-neck round bottom Schlenk-flask, sodium (2.23 g, 0.096 mmol) was dissolved in 150 mL liquid NH_3 at -70˚C. Finely-ground selenium (3.83 g, 0.048 mmol) was then added in portions. The reaction mixture was stirred for an additional 30 min at -70˚C and then allowed to warm up slowly. The obtained residue was dried in vacuo to afford 6.03 g (100%) Na_2Se as a highly air and moisture sensitive off-white solid. This was used without further purification.

SI 1.3 Chemical removal and *in vitro* reconstitution of the cubane cluster of HYDA1[4Fe4X]$_H$.

The [4Fe$_H$] cubane cluster was removed by chemical denaturation of the protein and chelation of the released iron atoms. The protein (200 µM) was anaerobically diluted 1:1 with 500 mM EDTA and again with 14 M urea to unfold the protein backbone in a procedure similar to that previously described by Mulder et al. (2009). The loss of enzymatic activity over time was analyzed by measuring specific di-hydrogen production in a standard methyl viologen assay upon addition of [2Fe$_H$]^{MIM}. Once enzyme activity was no longer detectable, the protein was purified using a desalting column. SDS-PAGE was performed to analyze protein quality. [4Fe4X]$_H$ (X = S, Se) was reconstituted overnight with slight modifications to the Mulder et al (2009) procedure, using a HEPES buffer (50 mM HEPES, pH 7, 300 mM NaCl, 20 % glycerol) supplemented with 10 mM DTT and 2 mM sodium dithionite

(NaDT).[4] 10 µM HYDA1[ΔH], without any inorganic cofactor, was reconstituted by adding iron(III)chloride to a final concentration of 1 mM, followed by 1 mM of disodium sulfide or 0.1 mM of disodium selenide. Reconstitution was followed by repetitive *in vitro* activity measurements, as described before for stripping. The reconstituted HYDA1[4Fe4X]$_H$ variants were purified by reverse anion exchange chromatography, using 1 M NaCl in the buffer.[5] After purification, the protein was concentrated using an Amicon Ultra centrifugal filter unit (MWCO 30 kDa), desalted into a Tris-HCl pH 8 buffer (100 mM) with 2 mM NaDT and further concentrated to 0.5-1 mM.

SI 1.4 [FeFe]-hydrogenase activity measurements.

For activity assays, 10 nM [FeFe]-hydrogenase was used in a potassium phosphate buffer (pH 6.8) supplemented with 10 mM of the electron mediator methyl viologen (MV) and 100 mM NaDT as a sacrificial electron donor. Reaction mixtures were incubated for 20 min at 37°C if not stated otherwise and gaseous headspace was measured using gas chromatography as described previously.[3b, 6] Activity measurements of HYDA1[4Fe4X]$_H$ proteins were conducted after the addition of a 10-fold excess of [2Fe$_H$]^{MIM} to the reaction mixture.[2]

SI 1.5 Time dependent chalcogenide reconstitution of HYDA1[ΔH].

Analysis of time dependency for iron-chalcogenide reconstitution was performed as described for the *in vitro* reconstitution, except that reconstituted HYDA1[4Fe4X]$_H$ variants were not purified prior to activity measurements. Small scale reaction mixtures of 20 µl were incubated at room temperature for 70 h and H_2 evolution activity was measured at various time points after adding a 10-fold excess of [2Fe$_H$]^{MIM} as described above.

SI 1.6 Determination of reaction kinetics of reconstituted and *in vitro* maturated HYDA1[4Fe4X]$_H^{MIM}$.

Interaction kinetics of HYDA1[4Fe4X]$_H^{MIM}$ with soluble redox mediators were analyzed by performing H_2 production activity measurements at increasing concentrations of the particular redox mediator. For methyl viologen (MV) dependent activity, concentrations of 0, 2.5, 5,10, 20 and 40 mM were used, while for PETF dependent activity, concentrations were adjusted to 0, 2.5, 5, 10, 20 and 40 µM. NaDT concentration was set to 100 mM for the MV dependent assay and to 50 mM for measuring PETF dependent H_2 evolution activity as described earlier.[3b] Reaction mixtures were incubated for 15 min at 37°C with constant shaking. All measurements were performed at least in triplicate.

SI 1.7 Crystallography

Plate-shaped crystals grew after 7 days in a hanging drop vapor-diffusion experiment under anaerobic conditions at 277 K. A 1:1 mixture of HYDA1[4Fe4Se]$_H$ (10 mg/ml) and 0.1 M TrisHCl pH 7.0, 0.2 M NaCl, 18.5 % PEG 4000 buffer was used. Crystals were mounted into CryoLoops™ (Hampton Research), protected with paraffin oil and flash-frozen with liquid N_2 under anaerobic conditions. The presence of Se in the crystals was confirmed by measurements of the X-ray fluorescence spectrum and fluorescence-detected X-ray absorption around the Se-edge at 0.9786 Å. Collection of diffraction data took place at the beamline PXII of the SLS (Villigen, Switzerland) and the beamline ID-29 of the ESRF (Grenoble, France) at 100 K to obtain two datasets of the same crystal with incident beam wavelengths of 0.9786 Å and 1.0332 Å, respectively. Both datasets were processed with the space group $P3_221$ using the software package XDS[7] and scaled to the high energy dataset with XSCALE[7] and assigned identical sets of R_{free} reflections. As a structure of HYDA1[4Fe$_H$] with a resolution of 1.97 Å is available (PDB ID 3LX4)[8], we attempted refinement of our structures (resolution of 3.1 Å) with rigid body refinement and refinement of B factors only. To this end, chain A of the structure of HYDA1[4Fe$_H$] was superposed to a recent structure of HYDA1[4Fe$_H$] from our group in space group $P3_221$ (unpublished), all B factors were set to 110 and the occupancy of all atoms of the [4Fe$_H$] cluster was set to 0 to avoid model bias in this region. This structure was used as a starting model for three cycles of rigid body and B factor optimization with the high energy dataset using the program phenix.refine[9]. Obvious differences between electron density and model were corrected manually with the help of the program Coot[10] (41 of 411 residues) and a second set of three rigid body and B factor optimization cycles was performed. In the resulting model, the occupancy of the [4Fe$_H$] atoms was set to 1, S atoms of the [4Fe$_H$] cluster were replaced by Se atoms, as were the S atoms in the restraint file for the cluster. This modified model with [4Fe4Se]$_H$ cluster was used to run another set of rigid body and B factor refinements with either the high energy or the low energy dataset. From these final models, density maps of the anomalous signal were calculated and a difference density of the two maps was determined using the program Coot. The anomalous signal was not used during any of the refinement steps. Refinement of the model with more degrees of freedom was attempted during several stages of the process, but always led to an increase in R_{work} and R_{free}. It should be noted that R_{free} is slightly smaller than R_{work} for the final high energy model (see Tab. S2). However, inheritance of the R_{free} set of the starting model (PDB ID 3LX4) was prohibited by a slightly different orientation of the molecules within the unit cell in our crystals and the crystals of Mulder et al. (2009) as demonstrated by the different space groups. As the models were only refined using rigid body fit and B factor optimization (the latter were not inherited from the starting model), we regard overfitting against information obtained from the starting model a minor problem. Independent from the R_{free} set, the predictive power of the chosen set of phases is demonstrated by the electron density of residues 201-203 (not present in the starting model) and the meaningful density derived from the anomalous signal, which was not included in any refinement step.

SI 1.8 FTIR measurements of chalcogenide reconstituted and *in vitro* maturated HYDA1[4Fe4X]$_H^{MIM}$.

HYDA1[4Fe4X]$_H$ and HYDA1[4Fe$_H$] were maturated *in vitro* with [2Fe$_H$]^{MIM} and concentrated to ~150-420 µM in 100 mM potassium phosphate buffer (pH 6.8) with 2 mM NaDT as described previously.[2] The enzymes were flushed either with 100% CO for 15 min to set the distinct H_{ox}-CO state [2b, 11] or with 100% N_2 for 30 min to obtain a mixture of redox states within the sample. Additionally, HYDA1[4Fe4Se]$_H^{MIM}$ and HYDA1[4Fe$_H$]^{MIM} samples were oxidized by addition of a 3-fold molar excess of thionine to set the defined H_{ox}-state. FTIR measurements were performed on a Bruker Vertex 70V spectrometer (BrukerOptics, Ettlingen, Germany) equipped with a nitrogen cooled mercury cadmium telluride detector. 10µl of the protein samples were injected in a MIU (manual injection unit, Micro-Biolytics, Esslingen, Germany) transmission cell and 1,500 scans for HYDA1[4Fe$_H$]^{MIM} and 2,900 scans for both HYDA1[4Fe4X]$_H^{MIM}$ variants were coadded for one spectrum. The measurements were carried out at 288 K with a spectral resolution of 2 cm^{-1} and a scanner velocity of 60 kHz. Scans were performed in double-sided forward–backward mode and the resulting interferograms were apodized with the Blackman-Harris three-term function with a zero filling factor of 4. Reference spectra were measured from buffer filled cell and the resulting absorbance spectra were evaluated using OPUS software 6.0 (Bruker).

SI.2 Enzyme kinetics of HYDA1[4Fe4X]$_H^{MIM}$ and HYDA1[4Fe$_H$]^{MIM}

SI 2.1 Methyl viologen and PETF specific enzyme kinetics

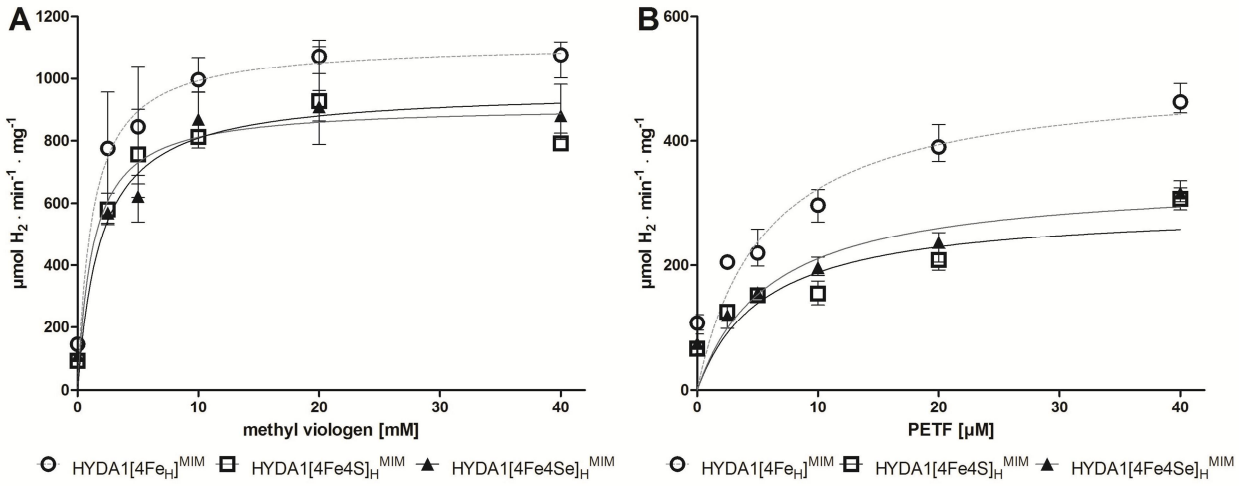

Figure S1. Michaelis-Menten kinetics of mediator-specific H_2 evolution activity for the reconstituted HYDA1[4Fe4X]$_H^{MIM}$ holoenzymes compared to wild type HYDA1[4Fe$_H$]^{MIM}. Hydrogen production activities were measured upon addition of increasing concentrations of either methyl violgen or PETF to 10 nM of *in vitro* maturated and chemically reconstituted (HYDA1[4Fe4X]$_H^{MIM}$) or recombinant hydrogenase (HYDA1[4Fe$_H$]^{MIM}). For methyl viologen dependent experiments, 100 mM sodium dithionite was used, while for PETF kinetics, NaDT concentration was set to 50 mM. All measurements were performed in triplicate and error bars represent standard deviation. Lines show fits to the experimental data calculated with GraphPad Prism® using the computationally intensive, iterative approach for nonlinear regression.

Table S1. Kinetic parameters for methyl viologen and PETF mediated hydrogen production activities of reconstituted HYDA1[4Fe4X]$_H^{MIM}$ and *E. coli* expressed HYDA1[4Fe$_H$]^{MIM}.[a]

		HYDA1[4Fe$_H$]^{MIM}	HYDA1[4Fe4S]$_H^{MIM}$	HYDA1[4Fe4Se]$_H^{MIM}$
methyl viologen	v_{max} [µmol H_2 · min^{-1} · mg^{-1}]	1115 ± 54	914 ± 43	965 ± 39
	K_m [mM]	1.23 ± 0.37	1.26 ± 0.37	1.93 ± 0.4
PETF	v_{max} [µmol H_2 · min^{-1} · mg^{-1}]	505 ± 44	294 ± 38	340 ± 32
	K_m [µM]	5.56 ± 1.58	5.62 ± 2.2	6.12 ± 1.82

[a]Values for the kinetic parameter K_m and V_{max} were calculated with GraphPad Prism® and are presented with standard deviations.

SI.3 Supplemental data from crystallography and FTIR of HYDA1[4Fe4Se]$_H$

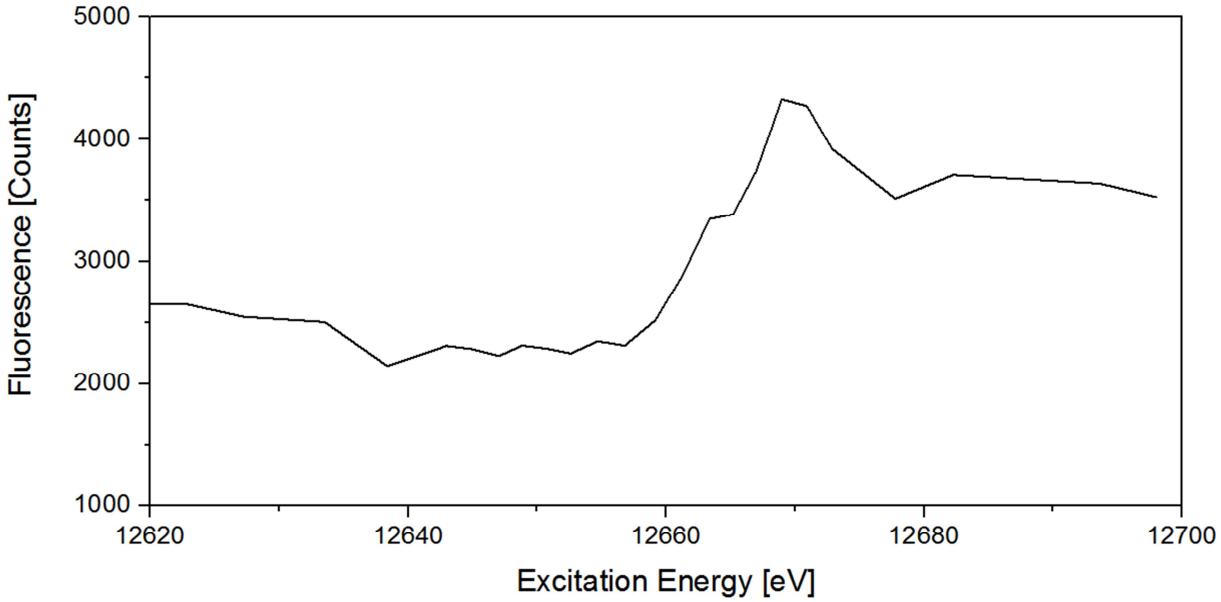

Figure S2: X-ray absorption edge scan of the HYDA1[4Fe4Se]$_H$ crystal. X-ray fluorescence of the HYDA1[4Fe4Se]$_H$ crystal while scanning over different excitation energies around the theoretical K-edge of X-ray absorption for Se at 12666 eV.

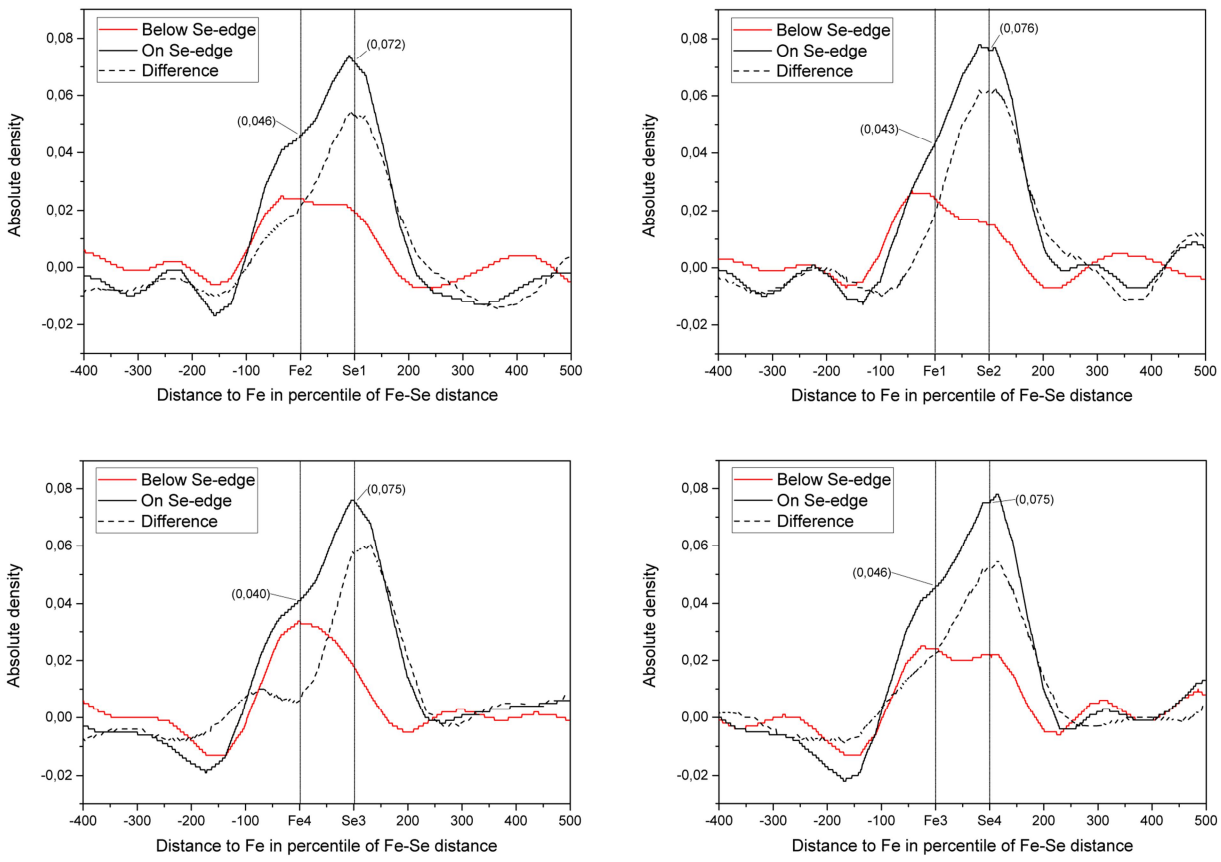

Figure S3: Densities of anomalous scattering maps on the atoms of the [4Fe4Se]$_H$ cluster. Densities of F(+)-F(-) anomalous scattering maps calculated from diffraction datasets of one HYDA1[4Fe4Se]$_H$ crystal taken on the Se-edge at 12669 eV (black solid lines) and below the Se-edge at 12000 eV (red solid lines) and densities of the difference map between the high energy dataset and the low energy dataset (black dashed lines) as used in Figure 3. For each set of Fe and Se atoms (indicated in the x-axes), densities were taken from a line through the atoms' positions as given in the calculated structure of HYDA1[4Fe4Se]$_H$ in steps of 1/100 of the Fe-Se distance. Absolute values of density at the centers of the Fe and Se atoms are given in the plots in parenthesis.

Table S2. Statistical data of the HYDA1[4FeSe]$_H$ crystal structure.

	HYDA1[4Fe4Se]$_H$- 12.000 keV	HYDA1[4Fe4Se]$_H$- 12.669 keV
Wavelength (Å)	1.033	0.9786
Resolution range (Å)	47.68 - 3.1 (3.21 - 3.1)	47.68 - 3.1 (3.21 - 3.1)
Space group	P 32 2 1	P 32 2 1
Unit cell	70.52 70.52 152.57 90 90 120	70.52 70.52 152.57 90 90 120
Total reflections	154828 (15093)	314707 (31622)
Unique reflections	8439 (826)	8439 (826)
Multiplicity	18.3 (18.3)	37.3 (38.3)
Completeness (%)	100.00 (100.00)	100.00 (100.00)
Mean I/sigma(I)	16.2 (2.0)	19.1 (1.8)
Wilson B-factor	89.6	108.5
R-merge	0.170 (1.5)	0.223 (2.5)
R-meas	0.175	0.226
CC1/2	0.99 (0.62)	0.999 (0.64)
CC*	1 (0.88)	1 (0.88)
Reflections used for R-free	422	422
R-work	0.22 (0.33)	0.22 (0.32)
R-free	0.22 (0.37)	0.22 (0.33)
Number of non-hydrogen atoms	3147	3147
macromolecules	3138	3138
ligands	9	9
water	0	0
Protein residues	413	413
RMS(bonds)	0.008	0.008
RMS(angles)	1.14	1.14
Ramachandran favored (%)	95	95
Ramachandran allowed (%)	0	0
Ramachandran outliers (%)	2	2
Clashscore	17.21	17.05
Average B-factor	86.6	108.1
macromolecules	86.6	108.1
ligands	80.9	111.7

Table S3: FTIR wavenumbers of $[2Fe_H]^{MIM}$ CO and CN^- frequencies assigned to different redox states of the selenium reconstituted HYDA1[4Fe4Se]$_H^{MIM}$ H-cluster.[b]

Redox state	HYDA1[4Fe4Se]$_H^{MIM}$ (wavenumber / cm^{-1})	Reference 12 (wavenumber / cm^{-1})
H_{ox}-CO	2092, *2082*, **2013**, ***1969*, 1964, 1810**	2092, 2084, 2013, 1970, 1964, 1810
$H_{'red'}$-CO	2086, 2075, ***2003***, 1967, 1951, 1793	2086, 2075, 2002, 1967, 1951, 1793
H_{ox}	2088, 2072, 1964,**1940**, 1800	2088, 2072, 1964, 1940, 1800
H_{red}	2088, 2072, **1935**, ***1892***, **1793**	2088, 2072, 1935, 1891, 1793
H_{sred}	2070, **2026**, ***1953***, **1919**, ***1883***	2070, 2026, 1954, 1919, 1882

[b]The spectra were measured at 288 K in 100 mM potassium phosphate buffer (pH 6.8) and do not differ significantly from those reported in [12] (right column). Bold numbers mark the most prominent bands which can be referred without doubt to the indicated state in the different samples shown in Fig. 3. All deviations to earlier FTIR-measurements (corresponding signals are presented in italic letters) are $\leq 2cm^{-1}$ and thus are in the range of standard deviation for FTIR-spectroscopy. These small shifts likewise concern the same bands of both protein, HYDA1[4Fe4Se]$_H^{MIM}$ and HYDA1[$4Fe_H$]^{MIM}.

References

[1] M. K. Akhtar, P. R. Jones, *Appl. Microbiol. Biotechnol.* **2008**, *78*, 853-862.

[2] a) G. Berggren, A. Adamska, C. Lambertz, T. R. Simmons, J. Esselborn, M. Atta, S. Gambarelli, J. M. Mouesca, E. Reijerse, W. Lubitz, T. Happe, V. Artero, M. Fontecave, *Nature* **2013**, *499*, 66-69; b) J. Esselborn, C. Lambertz, A. Adamska-Venkatesh, T. Simmons, G. Berggren, J. Noth, J. Siebel, A. Hemschemeier, V. Artero, E. Reijerse, M. Fontecave, W. Lubitz, T. Happe, *Nat. Chem. Biol.* **2013**, *9*, 607-609.

[3] a) J. Jacobs, S. Pudollek, A. Hemschemeier, T. Happe, *FEBS Lett.* **2009**, *583*, 325-329; b) J. Noth, D. Krawietz, A. Hemschemeier, T. Happe, *J. Biol. Chem.* **2013**, *288*, 4368-4377.

[4] D. W. Mulder, D. O. Ortillo, D. J. Gardenghi, A. V. Naumov, S. S. Ruebush, R. K. Szilagyi, B. Huynh, J. B. Broderick, J. W. Peters, *Biochemistry* **2009**, *48*, 6240-6248.

[5] J. L. Busch, J. L. Breton, B. M. Bartlett, R. James, E. C. Hatchikian, A. J. Thomson, *Biochem. J.* **1996**, *314 (Pt 1)*, 63-71.

[6] H. Krassen, S. Stripp, G. von Abendroth, K. Ataka, T. Happe, J. Heberle, *J. Biotechnol.* **2009**, *142*, 3-9.

[7] W. Kabsch, *Acta Crystallogr., Sect. D: Biol. Crystallogr.* **2010**, *66*, 125-132.

[8] D. W. Mulder, E. S. Boyd, R. Sarma, R. K. Lange, J. A. Endrizzi, J. B. Broderick, J. W. Peters, *Nature* **2010**, *465*, 248-251.

[9] P. V. Afonine, R. W. Grosse-Kunstleve, N. Echols, J. J. Headd, N. W. Moriarty, M. Mustyakimov, T. C. Terwilliger, A. Urzhumtsev, P. H. Zwart, P. D. Adams, *Acta Crystallogr., Sect. D: Biol. Crystallogr.* **2012**, *68*, 352-367.

[10] P. Emsley, B. Lohkamp, W. G. Scott, K. Cowtan, *Acta Crystallogr., Sect. D: Biol. Crystallogr.* **2010**, *66*, 486-501.

[11] A. Adamska, A. Silakov, C. Lambertz, O. Rüdiger, T. Happe, E. Reijerse, W. Lubitz, *Angew. Chem. Int. Ed. Engl.* **2012**, *51*, 11458-11462.

[12] A. Adamska-Venkatesh, D. Krawietz, J. Siebel, K. Weber, T. Happe, E. Reijerse, W. Lubitz, *J. Am. Chem. Soc.* **2014**, *136*, 11339-11346.